

1 **The unusual wet summer (July) of 2014 in Southern Europe**

2
3 **Satyaban B. Ratna, J. V. Ratnam, Swadhin K. Behera,**

4 Application Laboratory, Japan Agency for Marine-Earth Science and Technology, Yokohama 236-0001, Japan

5 **Annalisa Cherchi**

6 Centro Euro-Mediterraneo sui Cambiamenti Climatici and Istituto Nazionale di Geofisica e Vulcanologia, Bologna,

7 Italy

8 **Wanqiu Wang**

9 ³Climate Prediction Center, NOAA/NWS/NCEP, College Park, Maryland, USA

10 **Toshio Yamagata**

11 Application Laboratory, Japan Agency for Marine-Earth Science and Technology, Yokohama 236-0001, Japan

12
13
14
15
16
17
18
19
20
21 **Corresponding author**

22 Satyaban Bishoyi Ratna

23 Application Laboratory, JAMSTEC

24 Yokohama Institute for Earth Sciences

25 3173-25 Showa-machi, Kanazawa-ku, Yokohama

26 Kanagawa, 236-0001, Japan

27 Email: satyaban@jamstec.go.jp

28 Tel: +81-45-778-5515; Fax: +81-45-778-5497

31
32
33
34
35
36
37
38
39
40
41
42
43
44
45
46

Abstract

Southern Europe (Italy and the surrounding countries) experienced an unusual wet summer in 2014. The monthly rainfall in July 2014 was 84% above (more than three standard deviation) normal with respect to the 1982-2013 July climatology. The heavy rainfall damaged agriculture, and affected tourism and overall economy of the region. In this study, we tried to understand the physical mechanisms responsible for such abnormal weather by using model and observed datasets. The anomalously high precipitation over Italy is found to be associated with the positive sea surface temperature (SST) and convective anomalies in the tropical Pacific through the atmospheric teleconnection. Rossby wave activity flux at upper levels shows an anomalous tropospheric quasi-stationary Rossby wave from the Pacific with an anomalous cyclonic phase over southern Europe. This anomalous cyclonic circulation is barotropic in nature and seen extending to lower atmospheric levels, weakening the seasonal high and causing heavy precipitation over the Southern Europe. The hypothesis is verified using the National Centers for Environmental Prediction (NCEP) coupled forecast system model (CFSv2) seasonal forecasts. It is found that two-month lead forecast of CFSv2 was able to capture the wet summer event of 2014 over Southern Europe. The teleconnection pattern from Pacific to Southern Europe was also forecasted realistically by the CFSv2 system.

Key words: Wet summer; Southern Europe; Italy; Pacific Ocean; Sea surface temperature; teleconnection

47 **1. Introduction**

48 Southern Europe (Italy and neighboring countries) experienced an unusually wet and cold summer (June-
49 July-August) during 2014. Much of these regions were hit by severe storms, flooding and unusually chilly weather.
50 This unprecedented weather during the summer affected the socioeconomic conditions of these regions in terms of
51 agriculture and tourism. The unusual wet and cold conditions delayed the grape ripening and harvest had been
52 hindered that caused the Italian wine production fell by 15 percent as per the report of International Organization of
53 Vine and Wine (OIV, 2014). The cool and wet summer contributed a drop of 34% in the Italian olive oil production
54 according to International Olive Council (IOC, 2015). As per the report from the Food and Agriculture Organization
55 of the United Nations, heavy summer rainfall drenched some of France's key wheat-growing areas during this
56 summer (FAO, 2014). Entire tomato and lettuce fields also have been destroyed by persistent torrential rains.
57 The summer rain washed out family holidays and resulted in the loss of millions of euros in the tourism industry as
58 reported in several news media (Pasquaré and Venturini, 2016).

59 Southern Europe is the part of Mediterranean region that lies in a transition zone between the arid climate
60 of North Africa and the wet climate of central Europe. The transition zone climate is influenced by interactions
61 between mid-latitude and tropical processes (Raicich et al. 2003; Giorgi and Lionello, 2008). This region
62 experiences a hot, dry, sunny summer and a rainy winter season. In the boreal summer, the region is characterized
63 by descending motion (Raicich et al. 2003) and a minimum in seasonal rainfall (Mariotti et al. 2002). The
64 interannual variability of the circulation over the Atlantic-European sectors is affected by several teleconnections
65 such as the North Atlantic Oscillation (Hurrell, 1995; Kutiel et al. 1996; Brunetti et al. 2002; Zveryaev, 2004;
66 Folland et al. 2009), El Niño–southern oscillation (Fraedrich and Muller 1992; Dai et al. 1997; Trenberth et al. 1998;
67 Behera et al. 2013) and Asian summer monsoons (Rodwell and Hoskins 1996; Tyrlis et al. 2013; Cherchi et al.
68 2014). While it is the tropical sea surface temperature (SST) that most directly affects the overlaying large-scale
69 atmospheric circulations (Lau 1985; Lau and Nath 1994; Stern and Miyakoda 1995), atmospheric teleconnections
70 from the tropics to the extratropics may lead to some seasonal forecast skill in the extratropics via SST forcing of the
71 tropical atmosphere (Barnston 1994).

72 Due to its more northerly location and smaller spatial scale of the North Atlantic oscillation (NAO) during
73 the summer, its influence over the European climate diminishes compared to the winter counterpart (Folland et al.
74 2009). Also, due to the northward location of NAO during the summer season, the Mediterranean region is not under

75 the direct influence of the pressure anomalies associated with it and so its relationship with the Mediterranean
76 rainfall is small (Bladé et al. 2012). During July 2014, even though the NAO was weak with a slightly positive
77 (0.18) side
78 (<http://www.cpc.ncep.noaa.gov/products/precip/CWlink/pna/norm.nao.monthly.b5001.current.ascii.table>), southern
79 Europe experienced unusual excess rainfall. Also, the weak Asian monsoon can cause enhanced upward motion over
80 the Mediterranean region through monsoon-desert mechanism (Rodwell and Hoskins, 1996) and the Indian summer
81 monsoon in July 2014 was 10% below the normal. However, such negative Indian summer monsoon rainfall
82 anomaly had never caused such rainfall extreme over the Southern Europe. So, the persistent rainfall throughout
83 July is likely related to other teleconnections arising from large-scale climate variations or could be related with
84 internal variability. There are known difficulties in the prediction of boreal summer climate in mid-latitudes
85 (Zveryaev, 2004; Johansson et al. 1998; Colman and Davey, 1999; Dirmeyer et al. 2003) and so further detailed
86 analysis of the variability of summer climate is extremely important. The present study describes the exceptional
87 event and it also shows possible link of the event with the forcing from the sea surface temperature in the Pacific and
88 teleconnection patterns of the atmospheric circulation.

89 **2. Data and Methodology**

90 In this study, the abnormal high precipitation is verified using the monthly precipitation data from the
91 Global Precipitation Climatology Project version 2 (GPCP; Adler et al. 2003) and NOAA precipitation
92 reconstruction over the land (PREC/L; Chen et al. 2002) datasets. The GPCP data is available from 1979 and the
93 PREC/L data from 1948 and both datasets are available at 2.5 degrees horizontal resolution. The anomaly for these
94 data is generated from the climatology based on the period from 1982 to 2013. Apart from this, we also used
95 monthly TRMM 3B43 data (Huffman et al. 2007) available at 1-degree resolution for the verification of the event.
96 The daily variability of the precipitation during July 2014 is investigated with the aid of the GPCP daily data
97 (Huffman et al. 2001) at 1-degree resolution. The SST anomaly is derived from the National Oceanic and
98 Atmospheric Administration (NOAA) Optimum Interpolation sea surface temperature version 2 (OISSTv2;
99 Reynolds et al. 2002) available at 1 degree resolution. Monthly mean surface temperature, sea level pressure, along
100 with meridional and zonal wind data, and geopotential heights at various levels were taken from the Interim
101 European Centre for Medium-Range Weather Forecasts (ECMWF) Re-Analysis (ERA-Interim; Dee et al. 2011),
102 available at 1-degree spatial resolution.

103 In addition to the analysis based on observational data, we also investigate if a coupled general circulation
 104 model is able to represent the teleconnection that caused the excess rainfall over the Southern Europe. Here, we used
 105 the operational products from the NCEP climate forecast systems version 2 (CFSv2; Saha et al, 2006). The
 106 atmospheric component of CFS is the NCEP Global Forecast System model that has a spectral triangular truncation
 107 of 126 waves (T126) in the horizontal (equivalent to nearly a 100-km grid resolution) and a finite differencing in the
 108 vertical with 64 sigma-pressure hybrid layers. The oceanic component of CFSv2 is the NOAA Geophysical Fluid
 109 Dynamics Laboratory Modular Ocean Model (Griffies et al, 2004) version 4. The details of the model and its
 110 operational forecasts are described by Saha et al (2014).

111 The CFSv2 generates nine-month forecasts as a part of the seasonal prediction system and it is initialized
 112 four times per day (0000, 0600, 1200, and 1800 UTC). The CFSv2 forecast integrations cover the first partial month
 113 and nine full subsequent months into the future. In this study, we use the lagged ensemble of 40 forecast runs
 114 initialized from 21-30 April 2014 with four forecast members from each day. We diagnose forecast monthly mean
 115 fields of sea surface temperature, precipitation, and atmospheric data such as geopotential height, zonal and
 116 meridional winds at 200 hPa for July 2014, corresponding to a lead time of two months. As per the availability of
 117 CFS data, the anomalies are computed with respect to the 1999-2010 hindcast climatology.

118 The vertical motion and the associated low level convergence and upper level divergence induced by the
 119 equatorial sea surface temperature anomaly produce an anomalous vorticity source in the tropics. The upper level
 120 component of this vorticity source, denoted the Rossby wave source (RWS) by Sardeshmukh and Hoskins (1988),
 121 sets off a train of Rossby waves that comprise teleconnection patterns in the extratropics. As per Qin and Robinson
 122 (1993), the RWS is given by

$$\text{RWS} = \underbrace{-\mathbf{V}'_{\chi} \cdot \nabla(\bar{\zeta} + f)}_{(S1)} - \underbrace{(\bar{\zeta} + f)\nabla \cdot \mathbf{V}'_{\chi}}_{(S2)} - \underbrace{\zeta'\nabla \cdot \bar{\mathbf{V}}_{\chi}}_{(S3)} - \underbrace{\bar{\mathbf{V}}_{\chi} \cdot \nabla\zeta'}_{(S4)}$$

123 Where \mathbf{V}_{χ} is the rotational wind vector, ζ the relative vorticity and f the Coriolis parameter. $(\bar{\quad})$ and (\quad')
 124 represent the climatological mean and perturbation, respectively. The above equation is the breakdown of the full
 125 RWS (Sardeshmukh and Hoskins, 1988) into the tropical [$S1 + S4 (\approx S1)$] and extratropical parts ($S2 + S3 \approx S2$),
 126 which is instructive for evaluating the different roles played by these components in generating extratropical
 127 responses. It is found that S1 is more effective than S2 in exciting extratropical teleconnections (Sardeshmukh and
 128 Hoskins, 1988) and so in this study we calculated only S1 term to represent the RWS.
 129

130 **3. Results**

131 **3.1 Precipitation anomaly**

132 Southern Europe experienced very high precipitation during July of 2014. The precipitation anomaly
133 exceeding more than three standard deviations is seen over northern Italy and eastern France and Switzerland (Fig 1).
134 In addition, anomalous high precipitation is seen over the neighboring regions in Switzerland, France, Germany,
135 Austria, Slovenia, Croatia and western Hungary. The anomalous positive precipitation can be seen in all the datasets
136 analyzed in this study (Figure 1a, b, c) though variations in the magnitude of anomalies are noticed. The northern
137 Europe experienced below normal precipitation during the same period (Fig 1a, b). Due to the limitation of the
138 availability of the TRMM precipitation at latitudes higher than 50°N, the below normal precipitation over north
139 Europe is not seen in Fig 1c. It is reported that during July 2014 cities like Turin, Milan, Venice, Parma, Lucca in
140 Italy received 3 to 9 times more rainfall compared to the July climatology (Pasquaré and Venturini, 2016).
141 Analyzing the interannual variability of precipitation averaged over an area 3°E -18°E and 41°N - 50°N (box in
142 Figure 1a, b, c) over the period 1982-2014, it can be seen that Italy and surrounding regions received a record excess
143 of rainfall greater than 3 standard deviation (Fig. 1d) in July 2014, which is 84% higher compared to the July
144 climatology. This value is the highest in the study period of 33 years. This abnormal rainfall in July 2014 is also
145 highest during the past 114 years (1901-2014) in the Climate Research Unit (CRU; Harris et al. 2014) precipitation
146 dataset (not shown). The area averaged daily precipitation over the study domain shows high precipitation in almost
147 all the days of July 2014 compared to the climatological values (Fig 2a). The region received rainfall greater than
148 1mm/day for about 25 days in July 2014 (Fig 2b) out of which 8-10 days were having high amount (> 10 mm/day)
149 of rainfall. Climatologically, July is the month receiving the lowest seasonal rainfall in this region compared to the
150 other months of the year but the July 2014 was an abnormal month with anomalously high precipitation.

151 **3.2 Surface temperature and circulation anomaly**

152 The surface temperature anomalies during July 2014 show negative values (Fig 3a) over southern Europe
153 and low anomalies of mean sea level pressure (Fig 3b). On the other hand, northern Europe, which experienced
154 below normal precipitation, had large positive temperature anomaly (Fig 3a) with positive anomalies of sea level
155 pressure (Fig 3b). The 850 level geopotential height shows an anomalous low with a cyclonic circulation centered
156 over Italy. This low pressure and associated cyclonic circulation extends to the upper troposphere (200 hPa, Fig 3d),
157 indicating a clear barotropic nature. At the same time over northern Europe, sea level pressure anomalies are

158 characterized by a high with associated anticyclonic circulation extending from the surface to upper troposphere.
159 The above normal surface temperature associated with anticyclonic circulation over the Scandinavia region in the
160 northern Europe is caused by blocking in the atmosphere (Tyrlis et al, 2015). The atmospheric blocking plays an
161 important role in the mid-latitude climate variability and can be responsible for anomalous mean and/or extreme
162 climate. Dipole patterns of surface temperature and precipitation over Europe have been related to blocking (Behera
163 et al. 2013; Christensen et al. 2013; Sillmann and Croci-Maspoli, 2009; Masato et al. 2012, 2013) caused by the
164 quasi-stationary waves generated by SST anomalies in the Pacific Ocean (Behera et al. 2013). In the next section,
165 we see if similar processes were responsible for the precipitation anomaly in Europe during July 2014.

166 **3.3 Teleconnection**

167 To investigate the role of large scale processes that might have contributed to the anomalous low over
168 southern Europe during July 2014, we analyzed the global sea surface temperature and precipitation. The SST
169 anomalies in July 2014 were warmer than normal north of the equator throughout the Pacific Ocean (contour, Fig
170 4a). The SST anomalies were warmer than normal during this rather unusual El Niño year, when the warm signal
171 suddenly died after July to revive again in late autumn. A weak negative Indian Ocean Dipole (IOD; Saji et al. 1999)
172 also existed in the Indian Ocean during this time (Fig. 4a). A negative IOD can reduce monsoon rainfall over the
173 Indian sub-continent and this may lead to enhanced upward motion and wet condition over the Mediterranean region
174 through monsoon-desert mechanism (Rodwell and Hoskins, 1996). On the other hand, the enhanced monsoon
175 through a positive IOD can cause descent over the Mediterranean region (Guan and Yamagata, 2003). The tropical
176 and subtropical Pacific also received above normal precipitation (above 2 to 3 standard deviations) during July 2014
177 (shaded; Fig 4a). The abnormal precipitation is seen extending from west to east in the tropical Pacific and the
178 precipitation over the tropical Pacific Ocean (140⁰E-270⁰E; 5⁰N – 15⁰N) in July 2014 exceeded the July 1982-2013
179 climatology by 45%. Even the precipitation over Pacific is very high compared to the other years when the Pacific
180 Ocean was warmer than normal in July (not shown). This unusually strong convective activity and related
181 precipitation can induce climatic signal over remote areas through teleconnections.

182 The positive SST anomalies in the tropical Pacific (Fig 4a) in July 2014 have caused enhanced convection
183 and created upper level divergence (Fig 4b). This upper level divergence generates anomalous sources for the
184 Rossby waves (Sardeshmukh and Hoskins, 1988) through interaction with the upper level westerlies in the
185 subtropical regions. The anomalous tropical Rossby wave source (RWS) associated with the tropical heating is due

186 to the advection of the mean absolute vorticity by the anomalous divergent flow (Qin and Robinson, 1993). The
187 anomalous divergence at 200 hPa during July 2014 (Fig 4b) interacts with the westerlies in the subtropical region
188 (Fig 5a; contours) and generates an anomalous RWS in the region over subtropical eastern Pacific and mid-latitude
189 central-north Pacific (Fig 5a; shaded). To see if the quasi-stationary Rossby wave generated due to the anomalous
190 RWS affected the climate of southern Europe during July 2014, we calculated the wave activity flux (Takaya and
191 Nakamura, 2001). The anomalous wave activity flux originates from a source located in the subtropical eastern
192 Pacific (Fig 5b). It is noted that the surrounding region in the Pacific also received record rainfall during July 2014,
193 exceeding by about 70% to the 1982-2013 July climatology. The wave activity from this subtropical eastern Pacific
194 is seen as a major contributor to the anomalous quasi-stationary Rossby wave (vector, Fig 5b) reaching Europe,
195 though another minor source appears in the mid-latitude central-north Pacific, west of the dateline. The anomalous
196 quasi-geostrophic streamfunction also clearly shows a quasi-stationary wave from the eastern Pacific to the Europe
197 (shaded, Fig 5b). The spatial pattern of the generated anomalous Rossby wave train is such that it favors a cyclonic
198 circulation over Italy and its surrounding region (shaded, Fig 5b) reinforcing an anomalous equivalent barotropic
199 low there. We have also verified the wave train by analyzing the meridional wind anomaly (Fig. 5c) which shows
200 wave extending from the Pacific Ocean to Italy. Such mid-latitude circumglobal teleconnections during the Northern
201 Hemisphere summer are discussed in a few previous studies (Ding and Wang, 2005; Lin 2009; Yasui and Watanabe,
202 2010; Ding et al. 2011). The above analysis shows that the anomalies in the atmospheric convection/precipitation
203 caused upper level divergence, which on interaction with the upper level westerlies generated anomalous quasi-
204 stationary Rossby waves. The resulted anomalous cyclonic circulation resulted in higher than normal precipitation
205 over Italy in July 2014.

206 Given the understanding that the diabatic heating over the tropical Pacific is largely responsible for the
207 excess rainfall over southern Europe, we wanted to see if the event was predicted by the CFSv2 system. The
208 ensemble mean CFSv2 precipitation anomaly (Fig 6a) shows positive anomalies over southern Europe and negative
209 anomalies over north and northeast Europe, similar to the observed precipitation anomalies, though weaker in
210 magnitude. The CFS forecasts could capture the SST and convective anomalies over Pacific realistically (Fig. 6b).
211 The anomalous quasi-stationary wave from the Pacific to southern Europe was also captured realistically as seen
212 from the Rossby wave flux anomalies (Fig 6c) and the 200hPa meridional wind anomalies (Fig 6d).

213 On analyzing the individual members of the CFSv2 forecast, we found differences in the precipitation
214 anomalies over Southern Europe among the members. We compared those members by grouping the members that
215 forecasted wet July 2014 (hereafter ENSwet) against those ensemble members that forecasted dry July 2014
216 (hereafter ENSdry). A total of four members were found in each category. The forecast rainfall over Italy from the
217 ensemble mean of ENSwet and ENSdry are presented in Figure 7a, b. The differences between ENSwet and ENSdry
218 clearly shows positive rainfall anomaly over Italy region (Fig. 7c). The corresponding SST anomaly difference
219 between ENSwet and ENSdry shows positive anomaly over central, west and subtropical Pacific (Fig. 7f). It is seen
220 that ENSwet anomaly predicted excess rainfall over the Pacific Ocean compared to ENSdry (Fig. 7g, h) and the
221 difference is more over central Pacific north of the equator. This is the region for the source of Rossby waves
222 discussed in the observed analysis. Next, we plotted the meridional wind anomaly for the ENSwet and ENSdry to
223 check the differences in the wave from Pacific to Italy. It is seen that the simulated wave with ENSwet (Fig. 7j) is
224 clear and close to the observation. These differences in those two sets of ensemble forecasts further demonstrated
225 that the excess rainfall observed in the tropical and subtropical Pacific generated the Rossby wave to cause excess
226 rainfall over Italy. The CFSv2 forecast confirms the mechanism revealed by observational data and demonstrates
227 that the coupled model is capable of predicting the excess rainfall over southern Europe and associated
228 teleconnection from the Pacific.

229 **4. Summary**

230 In this study, we tried to understand the mechanism for the record high precipitation observed over
231 southern Europe (Italy and its surrounding region) during July 2014. To determine the processes responsible for the
232 rainfall and the associated cyclonic anomalies over Italy, we analyzed global observed SST, precipitation as well as
233 atmospheric circulation anomalies for this extreme summer. It is seen that the SST anomalies were anomalously
234 positive in the tropical Pacific during July 2014. Positive precipitation anomalies were also seen over the tropical
235 and subtropical Pacific. The corresponding upper level divergence over the subtropical Pacific generated an
236 anomalous Rossby wave source at 200hPa. The Rossby wave activity flux analysis demonstrated the anomalous
237 RWS and the associated Rossby wave extending from the Pacific to southern Europe. The phase of the generated
238 wave was such to favor cyclonic circulation over Italy and the surrounding countries. [We have reported this](#)
239 [relationship for the first time and we think that it could be an important factor for the extreme rainfalls over southern](#)
240 [Europe besides already known factors such as monsoon-desert mechanism, local phenomenon, blocking highs and](#)

241 other atmospheric internal variability. As the event described in the paper is unique for what we have found so far,
242 we cannot fully demonstrate the cause-effect relationship and identify it as a clear teleconnections. To fully assess a
243 direct cause-effect mechanism the event should be demonstrated using other observations or simulations, but the
244 lack of similar events in the available data is not sufficient for demonstrating the cause-effect relationship.

245 We also analyzed the excess rainfall over southern Europe and the teleconnection pattern from the NCEP
246 CFSv2 seasonal forecast. The CFSv2 captured the precipitation anomaly over Europe at the two-month lead time
247 with the positive anomaly over the southern Europe and negative anomaly over north and northeast Europe. The
248 model predicted the warm SST and excess rainfall over the subtropical Pacific similar to the observation. This
249 enhanced precipitation over the Pacific could have generated the Rossby wave through the diabatic heating in the
250 atmosphere, which can be seen from the wave activity flux. The CFSv2 model output is also analyzed by separating
251 the ensembles, which generated positive and negative rainfall anomalies over Italy. It is identified that the ensemble
252 members with wet anomaly over Italy also simulated wet anomalies in the subtropical Pacific compared to the
253 ensemble with dry anomaly over Italy. The ensembles with wet anomalies over Italy compared to dry ensembles
254 also simulated the wave realistically as in the observations.

255 The present study focuses on the mechanism for the unusual summer precipitation over southern Europe
256 during July 2014 on the possible link with the teleconnection patterns of the atmospheric circulation. Understanding
257 the observational links and relationship with the summer climate system may lead to an improved ability for
258 seasonal predictions of the European climate. More studies are desirable to analyze forecasts from other global
259 model forecast systems to see the fidelity of those models in predicting the observed extreme events.

260

261 **Acknowledgement:**

262 We are thankful to the two anonymous reviewers whose constructive comments helped improving the manuscript.
263 The authors are also thankful to the ECMWF for making available the ERA-Interim reanalysis datasets used in this
264 research. GPCP precipitation, PREC/L precipitation and NOAA OI SST data provided by the NOAA/OAR/ESRL
265 PSD, Boulder, Colorado, USA, from their Web site at <http://www.esrl.noaa.gov/psd/>.

266

267

268

269

270

271 **References**

- 272 Adler, R.F. et al, 2003. The Version 2 Global Precipitation Climatology Project (GPCP) monthly precipitation
273 analysis (1979–present). *J Hydromet.* 4:1147–1167.
- 274 Barnston, A.G., 1994. Linear statistical short-term climate predictive skill in the Northern Hemisphere, *J. Clim.* 7,
275 1513–1564.
- 276 Behera, S., Ratnam, J.V., Masumoto, Y., Yamagata, T., 2013. Origin of extreme summers in Europe: the Indo-
277 Pacific connection. *Clim Dyn.*, 41, 663 – 676.
- 278 Bladé. I., Liebmann, B., Fortuny, D., Oldenborgh, G.J., 2012. Observed and simulated impacts of the summer NAO
279 in Europe: implications for projected drying in the Mediterranean region. *Clim Dyn.* 39, 709–727.
- 280 Brunetti, M., Maugeri, M., Nanni, T., 2002. Atmospheric circulation and precipitation in Italy for the last 50 years,
281 *Int J Clim* 22, 1455–1471.
- 282 Chen, M., Xie, P., Janowiak, J.E., Arkin, P.A., 2002. Global Land Precipitation: A 50-yr Monthly Analysis Based
283 on Gauge Observations, *J. Hydromet.* 3, 249-266.
- 284 Cherchi, A., Annamalai, H., Masina, S., Navarra, A., 2014. South Asian Summer Monsoon and the Eastern
285 Mediterranean Climate: The Monsoon–Desert Mechanism in CMIP5 Simulations. *J. Clim.* 27, 6877–6903.
- 286 Christensen, J.H. et al 2013. Climate Phenomena and their Relevance for Future Regional Climate Change. In:
287 *Climate Change 2013: The Physical Science Basis. Contribution of Working Group I to the Fifth Assessment Report*
288 *of the Intergovernmental Panel on Climate Change*, Stocker, T.F., Qin, G.-K. Plattner, M. Tignor, S.K. Allen, J.
289 Boschung, A. Nauels, Y. Xia, V. Bex and P.M. Midgley (eds.). Cambridge University Press, Cambridge, United
290 Kingdom and New York, NY, USA
- 291 Colman, A., Davey, M., 1999. Prediction of summer temperature, rainfall and pressure in Europe from preceding
292 winter North Atlantic ocean temperature, *Int J Clim.* 19, 513–536.
- 293 Dai, A., Fung, I.Y., Del Genio, A.D., 1997. Surface observed global land precipitation variations 1900–88, *J. Clim.*
294 10, 2943–2962.
- 295 Dee, D.P., et al 2011. The ERA-Interim reanalysis: Configuration and performance of the data assimilation system.
296 *Quart. J. Roy. Meteor. Soc.* 137, 553–597.
- 297 Ding, Q., Wang, B., 2005. Circumglobal teleconnection in the Northern Hemisphere summer. *J Clim.* 18, 3483–
298 3505.

299 Ding, Q., Wang, B., Wallace, J.M., Branstator, G., 2011. Tropical-extratropical teleconnections in Boreal summer:
300 observed interannual variability. *J Clim.* 24,1878–1896.

301 Dirmeyer, P.A., Fennessy, M.J., Marx, L., 2003. Low skill in dynamical prediction of boreal summer climate:
302 Grounds for looking beyond sea surface temperature, *J. Clim.* 16, 995–1002.

303 FAO (Food and Agriculture Organization of the United Nations) 2014. Monthly news report on grains, MNR Issue
304 108: 1-12.

305 Folland, C.K et al., 2009. The summer North Atlantic Oscillation: past, present, and future. *J Clim.* 22, 1082–1103.

306 Fraedrich, K., Muller, K., 1992. Climate anomalies in Europe associated with ENSO extremes, *Int. J. Climatol.*, 12,
307 25–31.

308 Giorgi, F., Lionello, P., 2008. Climate change projections for the Mediterranean region. *Glo Plan. Chan.* 63, 90–
309 104.

310 Griffies, S. M., Harrison, M. J., Pacanowski, R. C. & Rosati, A., 2004. Technical guide to MOM4. GFDL Ocean
311 Group Technical Report No. 5, 337 pp. [Available online at www.gfdl.noaa.gov/~fms/.]

312 Guan, Z., Yamagata, T., 2003. The unusual summer of 1994 in East Asia: IOD teleconnections. *Geophys. Res. Lett.*,
313 30.1544, doi:10.1029/2002GL016831

314 Harris, I., Jones, P.D., Osborn, T.J., Lister, D.H., 2014. Updated high-resolution grids of monthly climatic
315 observations—the CRU TS3.10 dataset. *Int J Clim.* 34, 623–642.

316 Huffman, G.J. et al 2001. Global precipitation at one-degree daily resolution from multisatellite observations. *J.*
317 *Hydromet.* 2, 36–50.

318 Huffman, G.J. et al 2007. The TRMM Multi-satellite Precipitation Analysis: Quasi-global, multi-year, combined-
319 sensor precipitation estimates at fine scale. *J. Hydromet.* 8, 38–55.

320 Hurrell, J.W., 1995. Decadal trends in the Northern Atlantic oscillation — regional temperatures and precipitation.
321 *Science.* 269, 676–679.

322 Johansson, A., Barnston, A., Saha, S., Van den Dool, H. 1998. On the level and origin of seasonal forecast skill in
323 Europe, *J. Atmos. Sci.* 55, 103 – 127.

324 Kutie,l H., Maheras, P., Guika, S., 1996. Circulation and extreme rainfall conditions in the eastern Mediterranean
325 during the last century. *Int J Clim.* 16, 73–92.

326 Lau, N-C, Nath, M.J. 1994. A modeling study of the relative roles of the tropical and extratropical SST anomalies in
327 the variability of the global atmosphere-ocean system, *J. Clim.* 7, 1184 – 1207.

328 Lau, N-C., 1985. Modeling the Seasonal Dependence of the Atmospheric Response to Observed El Niños in 1962–
329 76. *Mon. Wea. Rev.* 113, 1970–1996.

330 Lin, H, 2009. Global extratropical response to diabatic heating variability of the Asian summer monsoon. *J Atmos*
331 *Sci.* 66, 2697–2713.

332 Mariotti, A., Struglia, M., Zengm N., Laum K-M,m 2002. The hydrological cycle in the Mediterranean region and
333 implications for the water budget of the Mediterranean Sea. *J. Clim.* 15, 1674–1690.

334 Masato, G., Hoskins, B.J., Woollings, T.J., 2012. Wave-breaking characteristics of midlatitude blocking. *Quart. J.*
335 *Roy. Meteor. Soc.* 138, 1285–1296.

336 Masato, G., Hoskins, B.J., Woollings, T.J., 2013. Wave-breaking characteristics of Northern Hemisphere winter
337 blocking: A two-dimensional approach. *J. Clim.* 26, 4535–4549.

338 OIC-International Olive Council 2015. Olive oils production data. Available at:
339 <http://www.internationaloliveoil.org/documents/viewfile/4246-production2-ang/>.

340 OIV-International Organisation of Vine and Wine 2014. Global economic vitiviniculture data. Press Release.
341 Available at: http://www.oiv.int/oiv/files/EN_Press_Release_OIV_23_October.pdf.

342 Pasquaré M, F., Venturini, C., 2016. 2014, The “year without a summer” in Italy: news media coverage and
343 implications for the climate change debate. *Environ Dev Sustain.* doi:10.1007/s10668-016-9805-8

344 Qin, J., Robinson, W.A., 1993. On the Rossby Wave Source and the Steady Linear Response to Tropical Forcing. *J.*
345 *Atmos. Sci.* 50, 1819–1823.

346 Raicich, F., Pinardi, N., Navarra, A., 2003. Teleconnections between Indian monsoon and Sahel rainfall and the
347 Mediterranean. *Int J Clim.* 23, 173–186.

348 Reynolds, R.W., Rayner, N.A., Smith, T.M., Stokes, D.C., Wang, W., 2002. An improved in situ and satellite SST
349 analysis for climate. *J. Clim.* 15, 1609–1625.

350 Rodwell, M.J., Hoskins, B.J., 1996. Monsoons and the dynamics of deserts. *Quart J Roy Meteor Soc* 122: 1385–
351 1404

352 Saha, S., & Coauthors., 2006. The NCEP Climate Forecast System. *J. Climate*, 19, 3483–3517

353 Saha, S., & Coauthors., 2014. The NCEP Climate Forecast System Version 2. *J. Climate*, 27, 2185–2208

354 Saji, H.N., Goswami, B.N., Vinayachandran, P.N., Yamagata, T.A., 1999. Dipole mode in the tropical Indian Ocean.
355 Nature. 401, 360-363.

356 Sardeshmukh, P.D., Hoskins, B.J., 1988. The Generation of Global Rotational Flow by Steady Idealized Tropical
357 Divergence. J. Atmos. Sci. 45, 1228–1251.

358 Sillmann, J., Croci-Maspoli, M. 2009. Present and future atmospheric blocking and its impact on European mean
359 and extreme climate. Geophys. Res. Lett., 36, L10702, doi:10.1029/2009GL038259.

360 Stern, W.F., Miyakoda, K., 1995. Feasibility of seasonal forecasts inferred from multiple GCM simulations. J. Clim.
361 8, 1071-1085.

362 Takaya, K., Nakamura, H.A., 2001. Formulation of a Phase-Independent Wave-Activity Flux for Stationary and
363 Migratory Quasigeostrophic Eddies on a Zonally Varying Basic Flow. J. Atmos. Sci. 58, 608-627.

364 Trenberth, K.E. et al 1998. Progress during TOGA in understanding and modeling global teleconnections associated
365 with tropical sea surface temperatures. J. Geophys. Res. 103, 14291-14324.

366 Tyrlis, E., Lelieveld, J., Steil, B., 2013. The summer circulation over the Eastern Mediterranean and the Middle
367 East: influence of the South Asian monsoon. Clim Dyn. 40, 1103–1123.

368 Tyrlis, E., Tymvios, F. S., Giannakopoulos, C., Lelieveld, J., 2015. The role of blocking in the summer 2014
369 collapse of Etesians over the eastern Mediterranean, J. Geophys. Res. Atmos. 120, 6777–6792.

370 Yasui, S., Watanabe, M., 2010. Forcing processes of the summertime circumglobal teleconnection pattern in a dry
371 AGCM. J Clim. 23.2093–2114

372 Zveryaev, I.I., 2004. Seasonality in precipitation variability over Europe. J Geophys Res 109 D05103, DOI
373 10.1029/2003JD003668

374

375

376

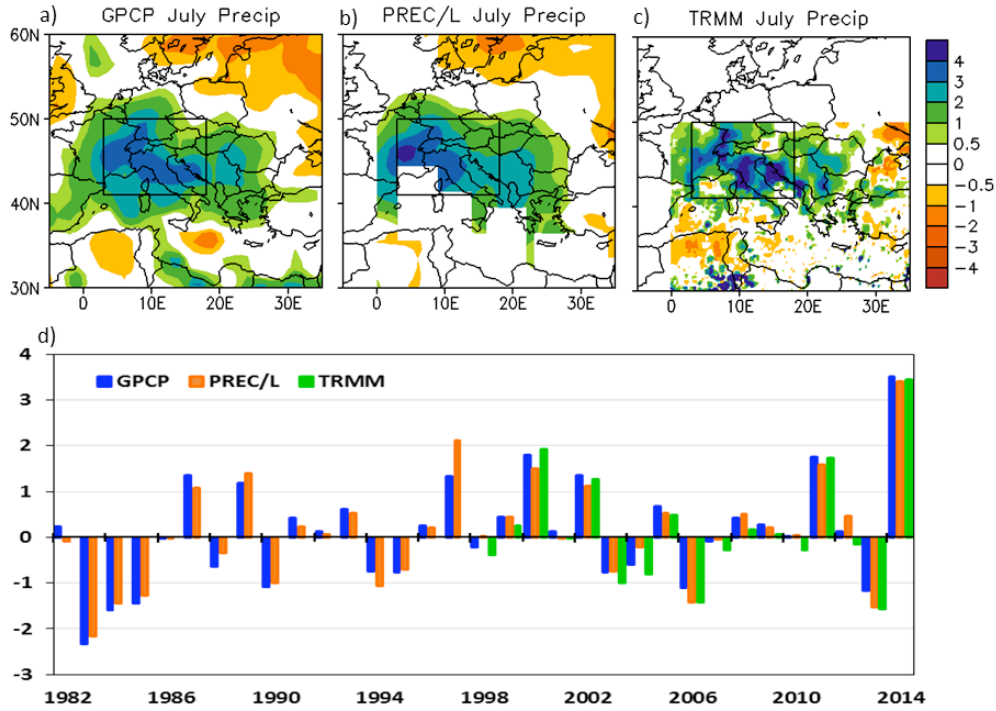
377

378

379

380

381



383

384

385 **Figure 1.** Standardized precipitation anomaly for July 2014 for (a) GPCP (b) PREC/L and (c) TRMM 3B43 data.

386 (d) Interannual variability of standardized precipitation anomaly (mm/day) averaged over the area 3°E – 18°E and

387 41°N-50°N (marked as a box in a, b and c) for July month during the period 1982-2014. TRMM data is available

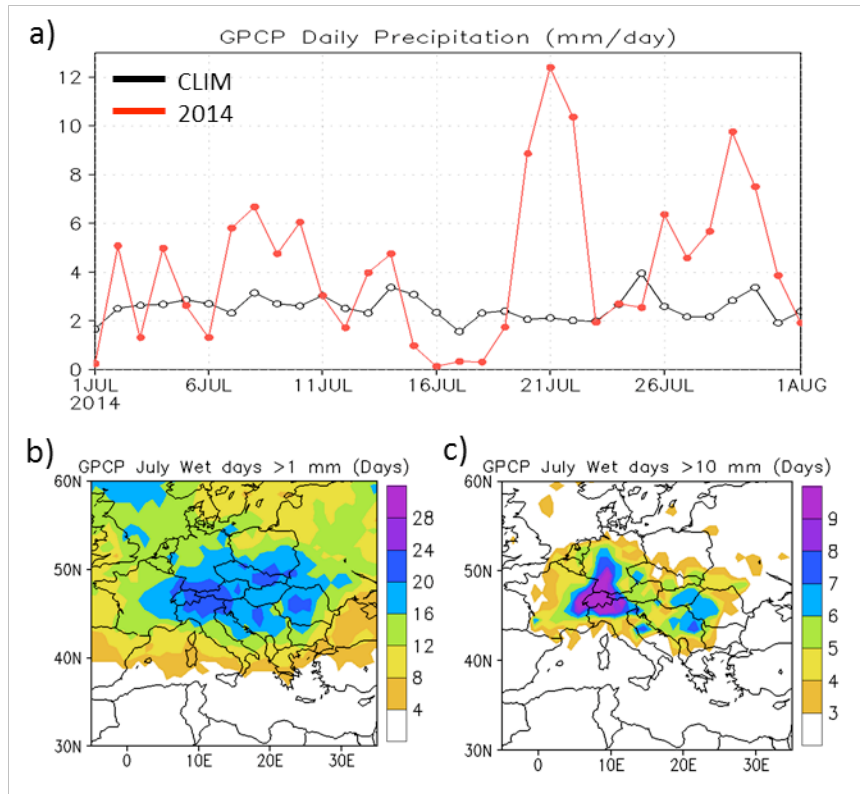
388 over the latitude band 50S-50N and for the period 1998-2014. The anomalies are calculated with respect to the July

389 climatology for the period 1982-2013 (1998-2013 for TRMM).

390

391

392



393

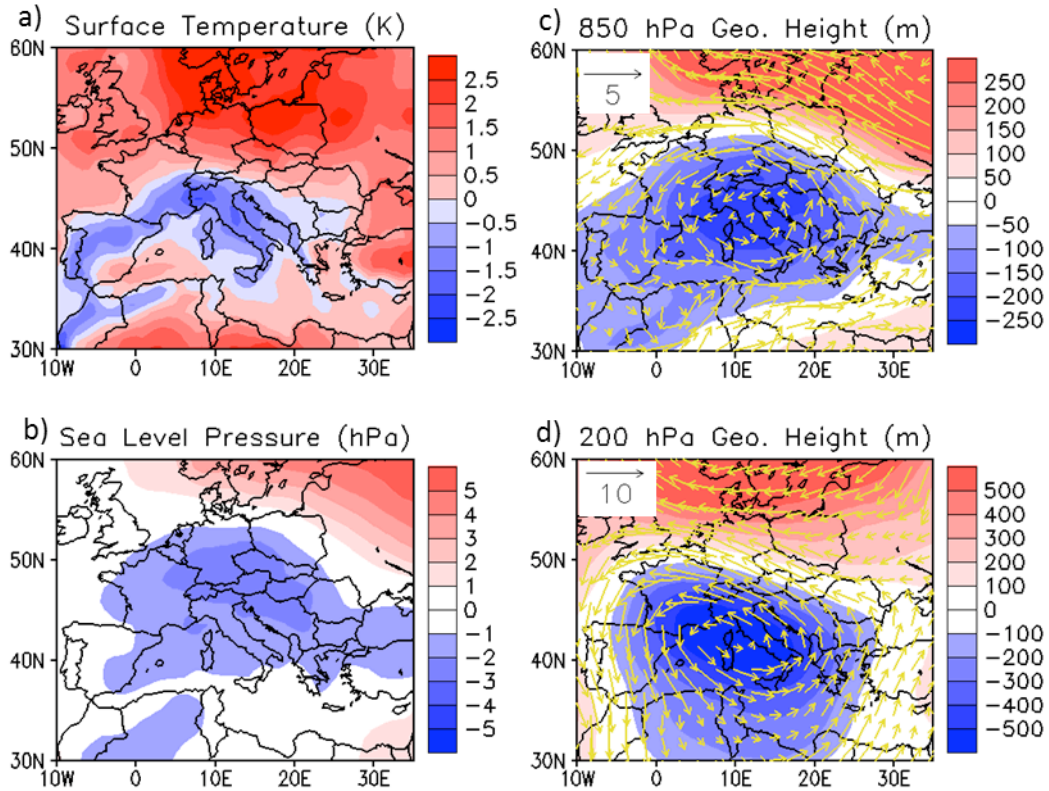
394 **Figure 2.** (a) Daily precipitation (mm/day) averaged over the area $3^{\circ}\text{N} - 18^{\circ}\text{N}$ and $41^{\circ}\text{N}-50^{\circ}\text{N}$ for July 2014 (red

395 line) and daily climatology for July (black line). (b) Number of wet days > 1 mm in July and (c) Number of wet days

396 > 10 mm in July. The climatology for the GPCP daily precipitation is obtained for the period 1997-2014.

397

398



400

401 **Figure 3.** (a) Surface temperature anomaly (K) for July 2014. (b) Same as (a) but for the sea level pressure (hPa).

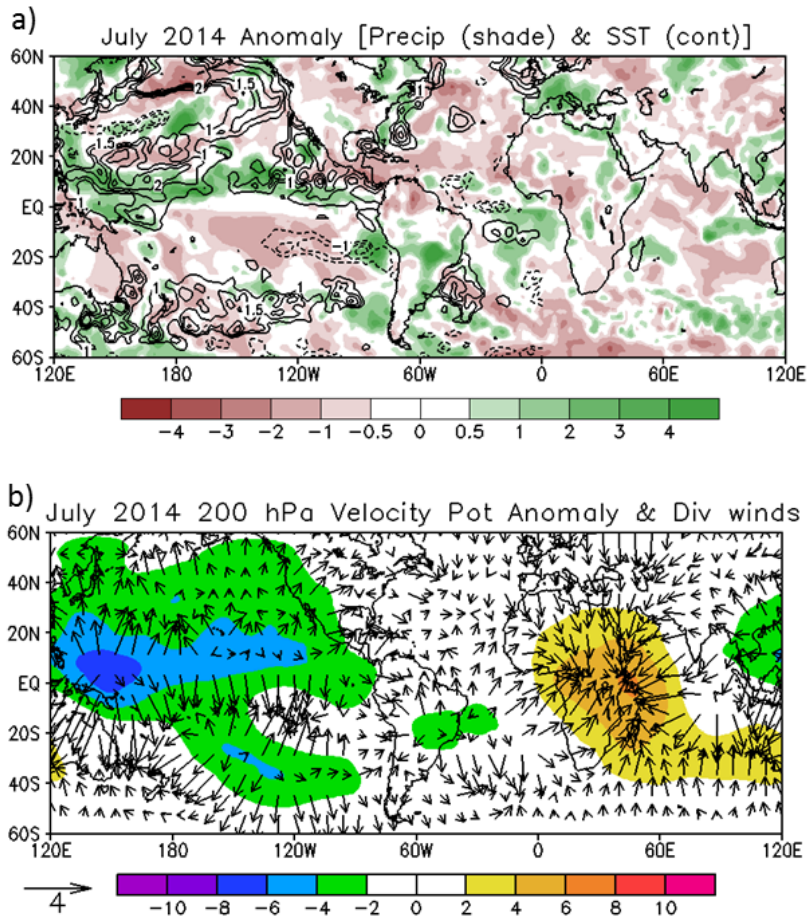
402 (c) Geopotential height (m) and wind vector (m/s) anomaly at 850 hPa level. (d) Same as (c) but for 200 hPa level.

403 All figures are with ERA-Interim data and the anomalies are calculated with respect to the July climatology for the

404 period 1982-2013.

405

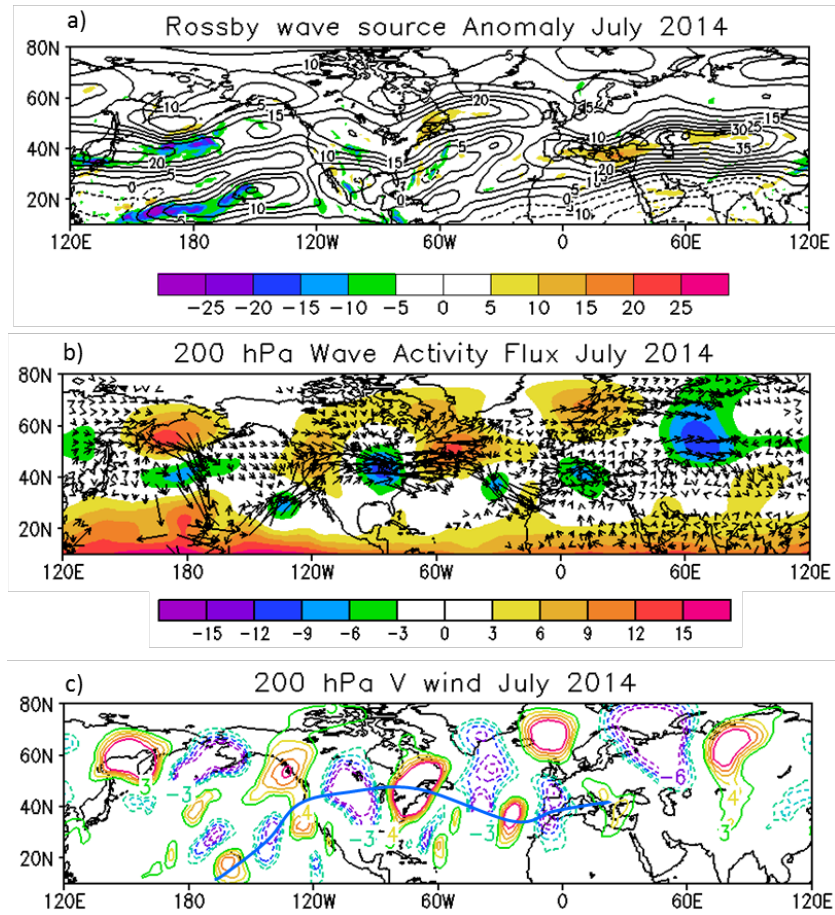
406



407

408 **Figure 4.** (a) Precipitation (mm/day, shaded) anomaly and sea surface temperature anomaly (K, contour) for July
409 2014 standardized with respect to 1982-2013 climatology. The contours for the SST are drawn at 1, 1.5, 2 and 2.5 K.
410 and (b) Velocity potential ($\times 10^6 \text{ m}^2 \text{ s}^{-1}$, shaded) and divergent component of winds (m s^{-1} , vectors) at 200 hPa for
411 July 2014.

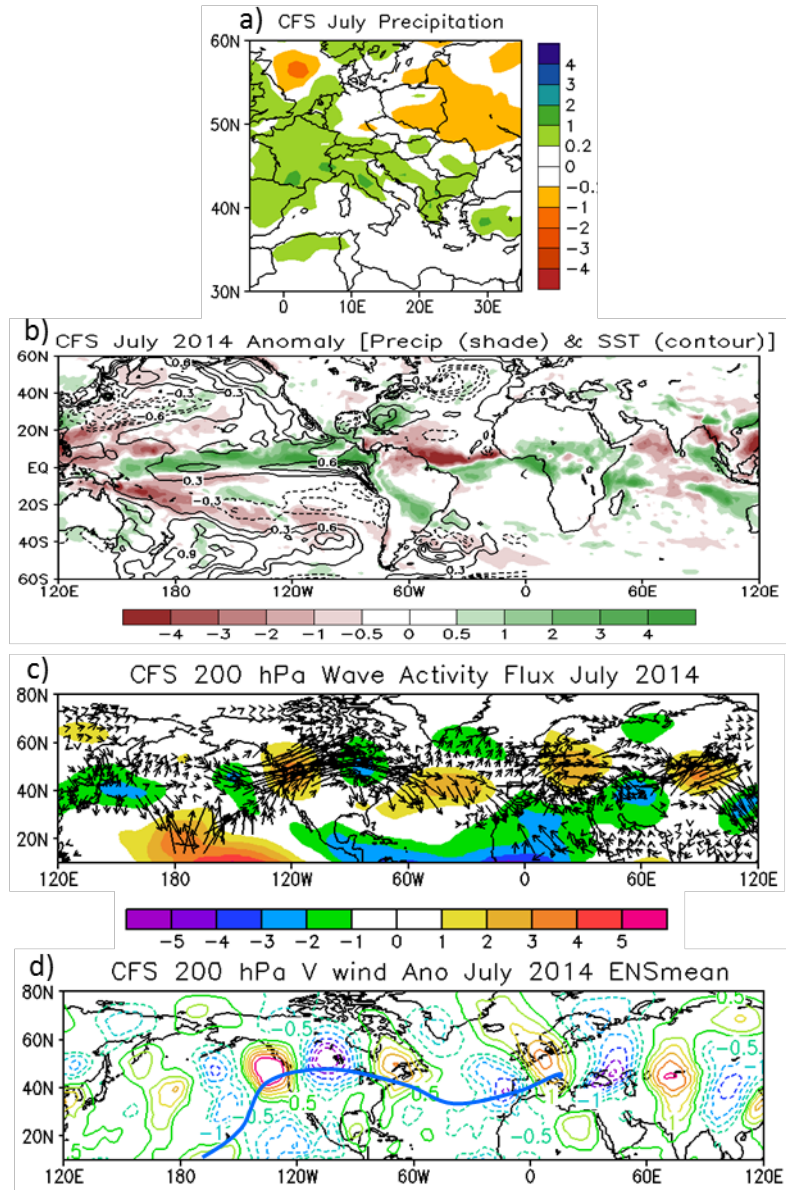
412



414

415 **Figure 5.** (a) Rossby wave source anomaly ($\cdot 10^{-11} \text{ s}^{-1}$, shaded) and zonal winds (m/s, contours) at 200 hPa for July
416 2014. The negative value of RWS is known as source. (b) Stream function anomaly ($\cdot 10^6 \text{ m}^2 \text{ s}^{-1}$ shaded) and wave
417 activity flux ($\text{m}^2 \text{ s}^{-2}$, vector) at 200 hPa level for July 2014. (c) 200 hPa meridional wind anomaly for July 2014.

418

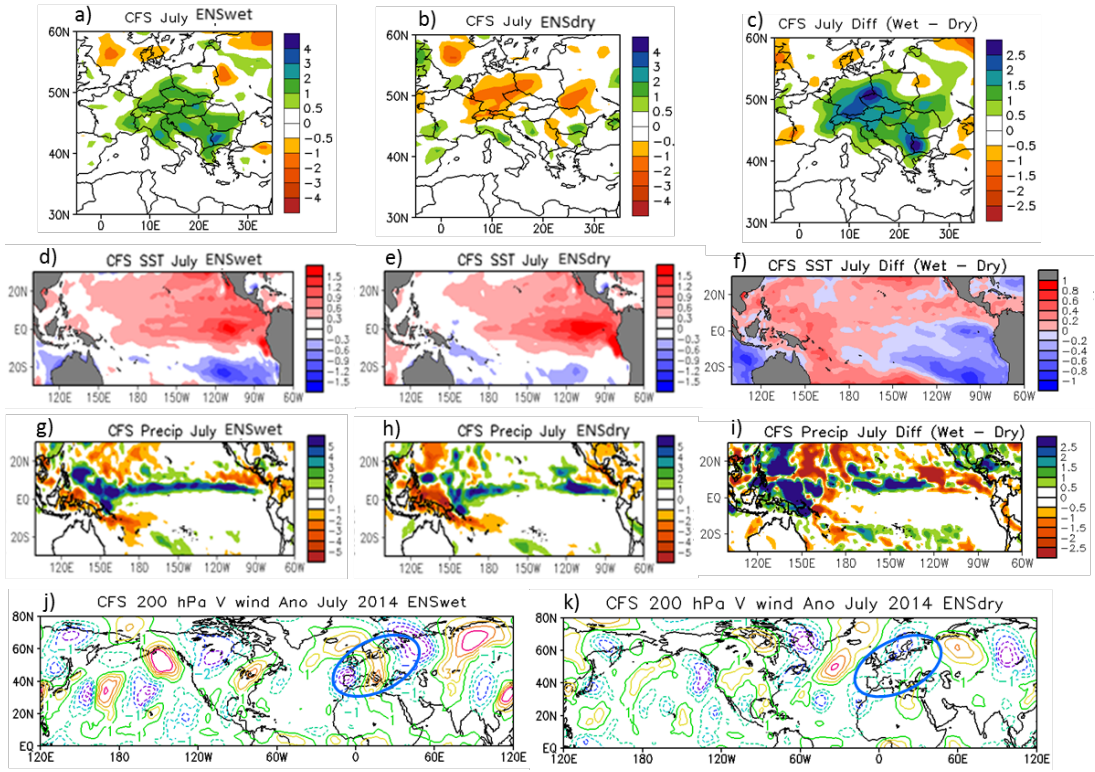


419

420 **Figure 6.** (a) CFS forecasted precipitation anomaly (mm/day) over Europe. (b) CFS forecasted Sea surface
 421 temperature anomaly (K, contour) and precipitation (mm/day, shaded) anomaly. (c) CFS forecasted stream function
 422 anomaly and wave activity flux at 200 hPa. (d) CFS forecasted 200 hPa meridional wind (m/s) anomaly for July
 423 2014.

424

425



426

427

428 Figure 7. Precipitation anomaly over South Europe for those ensembles that generated wet (ENSwet) and dry
 429 (ENSdry) anomalies over Italy. (a) ENSwet (b) ENSdry (c) difference between ENSwet and ENSdry. (d, e, f) same
 430 as (a, b, c) but for SST anomalies. (g, h, i) same as (a, b, c) but for precipitation anomalies. (j, k) 200 hPa meridional
 431 wind anomalies for ENSwet and ENSdry.